Using MetaPrisms for Performance Improvement in Wireless Communications

(Article begins on next page)

28 April 2024

Using MetaPrisms for Performance Improvement in Wireless Communications

Davide Dardari, *Senior Member, IEEE*, Devis Massari

Abstract—In this paper, we put forth the idea of *metaprism*, a passive and non-reconfigurable metasurface acting as a metamirror with frequency-dependent reflecting properties within the bandwidth of the signal. We show that, with an appropriate design of the metaprism, it is possible to control that each data stream in an orthogonal frequency division multiplexing (OFDM) system is reflected in the desired direction by properly assigning subcarriers to users without the need of control channels and dedicated channel state information (CSI) estimation schemes. Furthermore, the metaprism can also be designed so that it focuses the signal towards a specific position depending on the subcarrier, provided that the user is in the near-field region of the metaprism, with consequent path-loss reduction. A critical discussion is also presented about the path-loss reduction obtainable from metaprisms and, more generally, from metasurfaces. The numerical results show that this solution is effective in extending the coverage in areas experiencing severe non line-of-sight (NLOS) channel conditions, thus making it an interesting alternative to reconfigurable metasurfaces when low-cost, no energy consumption, and backward compatibility with existing wireless standards are required.

Index Terms—Metaprism; metasurfaces; intelligent surfaces; beamsteering; focusing; NLOS; near-field; spherical wavefront.

I. INTRODUCTION

THE exponential growth in traffic demand in wireless networks has forced the exploitation of new frequency bands in the millimeter wave region and, more in perspective, at THz frequencies [1], [2]. When switching to higher frequencies, on the one hand, more bandwidth is available but, on the other hand, the wireless channel suffers a higher path-loss and might be subjected to signal blockage when in the presence of obstacles. In fact, wireless communication relies mainly on the presence of the line-of-sight (LOS) direct path and of scarce multipath components [3]. This makes the coverage of NLOS areas more challenging than at lower frequency bands, where NLOS communication can be guaranteed by exploiting the rich multipath deriving from electromagnetic (EM) scattering, especially when using massive multiple-input multiple-output (MIMO) systems capable of "focusing" the multipath components on receiver's position [4]. As a matter of fact, there is a need for low-cost, energy-efficient solutions to extend the coverage without deploying additional base stations (BSs).

The introduction of metamaterials to realize, for instance, the so called *metasurfaces* has boosted a fertile research area [5]–[8]. In fact, with metasurfaces EM waves can be shaped almost arbitrarily to obtain a given functionality. Possible applications include, but are not limited to, transmitarrays [9], metamirrors [10]–[12], reflectarrays [13], [14], holograms [6], [15] and large intelligent surface (LIS) antennas to improve the communication capacity [16]–[20] or to enable single-anchor localization [21]. In addition, frequency-selective surfaces are used in dual-band reflectarrays [22], antenna covering surfaces, frequency-selective absorbers and, in general, to perform spectral filtering in both microwave and optical ranges through the design of metasurfaces with extremely dispersive reflection or transmission properties [6]. The recent availability of programmable metasurfaces to design smart EM reflectors using thin metamaterials has opened new very appealing perspectives [23], [24]. These reconfigurable intelligent surfaces (RISs) can be embedded in daily life objects such as walls and buildings. Environments coated with intelligent surfaces constitute the recently proposed *smart radio environments* concept [25], [26]. In smart radio environments, the design paradigm is changed from wireless devices/networks that adapt themselves to the environment (e.g., propagation conditions), to the joint optimization of both devices and environment using RISs. The advantages of RIS-enabled environments have been analyzed in several papers. For instance, in [27] a RIS-enhanced OFDM system is investigated, where the power allocation and the phase profile of the metasurface are jointly optimized to boost the achievable rate of a cell-edge user. In [28], it is shown how the rank of a MIMO communication in LOS can be increased by adding a RIS generating an artificial path. The authors in [29] present a comparison between RIS- and relay-enabled wireless networks by discussing the similarities and differences. Other studies can be found, for instance, in [30]–[32] and in the surveys [33], [34]. Despite being promising solutions, RIS-based systems have some disadvantages which could make them less appealing in some applications. In fact, to reconfigure a RIS in real-time, a dedicated control channel is needed which might entail a certain signaling overhead and, above all, additional complexity and cost. Moreover, a RIS needs to be powered and this might not be possible or convenient in many scenarios. A fundamental challenge when using a RIS is the estimation of the CSI [26], [33], [34]. In fact, the optimal configuration of the RIS's reflection coefficients, i.e., on how the RIS reflects the impinging EM wave, is a function of the state of the channel between the RIS and the BS as well as between the RIS and the mobile user (local CSIs). Its estimation is quite challenging because it may require additional hardware at the RIS to perform sensing
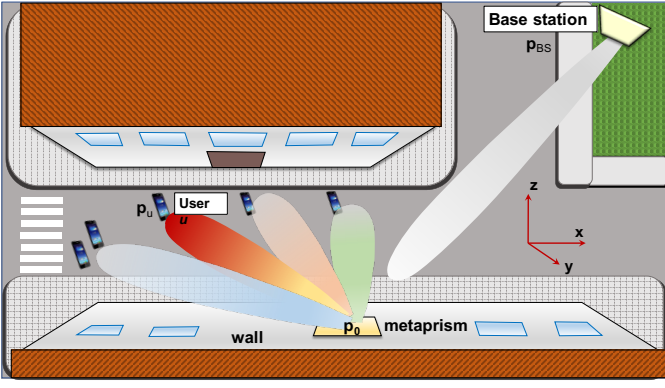
Fig. 1. The considered NLOS scenario empowered by a metaprism.

(semi-passive RIS) or ad hoc CSI protocols and methods [33], [35]. Regarding the latter, it has been shown that the estimation of the cascaded transmitter-RIS-receiver channel is sufficient for the end-to-end system optimization [35], [36]. However, the cascaded channel has a very large dimensionality, which may encompass hundreds or even thousands of channel co-efficients to be estimated, which may result in an excessive overhead, especially in dynamic networks. Once the reflection coefficients have been computed, they must be sent to the RIS through a dedicated control channel that should be established between the BS and the RIS. Finally, the RIS should be able to re-configure itself in a very short time in order to follow the dynamic changes in the propagation environment [33]. Even though some recent papers propose optimization algorithms based on statistical CSI (see for instance [37]), which in part relax the configuration speed of the RIS, the channel estimation in RIS-aided systems is still an open issue that is characterized by three major challenges: (i) the long training time, especially in multi-user MIMO systems, which may not be tolerable in dynamic scenarios; (ii) the real-time reconfiguration of the reflection functionality of the RIS through a dedicated control channel with the BS; and (iii) the need of ad hoc channel estimation and signaling protocols that make the introduction of RISs non-transparent to existing communication protocols. All these issues might in part vanish some of the main expected advantages of RISs, i.e., low-cost, low-complexity and low-energy consumption, making them less appealing with respect to conventional relays if not properly tackled [29].

In this paper, we introduce the novel idea of *metaprism*, a full passive and non-reconfigurable metasurface that acts as a metamirror, whose reflecting properties are frequency-dependent within the signal bandwidth. As already remarked, frequency-selective metasurfaces are not new but, to the knowledge of the Authors, this is the first paper proposing and analyzing how to exploit OFDM signals and frequency-selective reflecting metasurfaces with the purpose to improve the coverage of short-range wireless networks both in far-field and near-field channel conditions. A typical example of use-case scenario is shown in Fig. 1, where mobile users are in NLOS condition with respect to the BS and the metaprism is introduced to extend the covered area at a low-cost. Thanks

to the proposed metaprism, one can control the reflection of the signal through a proper selection of the subcarrier assigned to each user using a conventional OFDM signaling, without interacting with the metaprism and without the need of dedicated CSI estimation schemes, which are the main current challenges and drawbacks of RISs as previously outlined. We show that, with an appropriate design of the frequency-dependent phase profile of the metaprism, a significant path-loss reduction can be obtained by steering/focusing the signal towards/on a specific position depending on the assigned subcarrier. Specifically, we provide design criteria for the phase profile of the metasprism to obtain subcarrier-dependent beamsteering, when users are in the far-field region of the metaprism, as well as focusing when users are in the near-field region, thus exploiting the spherical wavefront EM propagation. In addition, we propose an example of a low-complexity subcarrier assignment algorithm capable of guaranteeing all the users with the same achievable rate. The numerical results corroborate the validity of the idea showing the significant performance improvement in wireless network coverage and achievable rate, making the metaprism an appealing alternative to RISs.

The remainder of this paper is organized as follows. In Section II, the frequency-dependent modeling of metasurface is introduced. The OFDM wireless link aided by metaprisms is characterized in Section III, whereas in Sections IV and V, the design criteria of phase profiles for the metaprism to realize, respectively, frequency-dependent beamsteering and focusing are elaborated. Some considerations about the validity of path-loss models when using metaprisms and, more in general, RISs are given in Section VI. An example of an algorithm to assign subcarriers in a multi-user scenario in order to equalize and maximize the per-user achievable rate is proposed in Section VII. Numerical results and discussions are presented in Section VIII. Finally, conclusions are drawn in Section IX.

II. FREQUENCY-SELECTIVE MODELS FOR METASURFACES

A. General Model

There are several technologies to realize a metasurface each of them obeys a specific model. A rough classification can be done between metasurfaces whose cells can be seen as small radiating elements with tunable load impedance [13], [38]–[40], i.e., using volumetric metamaterials with several wavelengths thick, and subwavelength metasurfaces producing a modification of the EM field which can be modeled as impedance sheets [6], [11], [41]–[43]. To facilitate the explanation and analysis, we focus on the first class even though the metaprism concept introduced in this paper can be applied to the second class as well. With reference to Fig. 2 (top), consider a metasurface in the $x - y$ plane with center at coordinates $\mathbf{p}_0 = (0, 0, 0)$, consisting of $N \times M$ cells of size $d_x \times d_y$ distributed in a grid of points with coordinates $\mathbf{p}_{nm} = (x_n, y_m, 0)$, where $x_n = n\, d_x - N\, d_x/2$, $n = 0, 1, \ldots N-1$, and $y_m = m\, d_y - M\, d_y/2$, $m = 0, 1, \ldots M-1$. The total surface's size is $L_x \times L_y$, with $L_x = N\, d_x$ and $L_y = M\, d_y$. The cell's size d_x, d_y, respectively, in the x and y directions, may be smaller than the wavelength λ, typically $d_x, d_y \approx \lambda/2 - \lambda/10$ [5], [7].
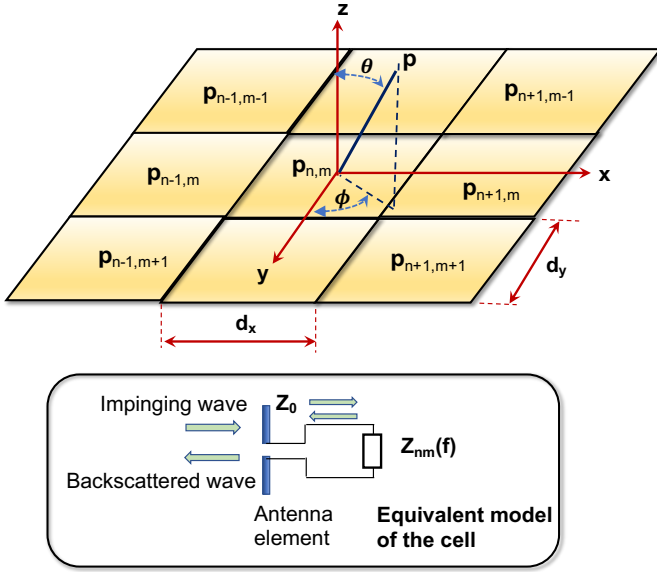
Fig. 2. Metasurface composed of elementary cells (top). Equivalent model of the cell (bottom).

A quite general equivalent model of the nmth cell of the metasurface at position $\mathbf{p}_{nm}$ is shown in Fig. 2 (bottom), which consists of a radiation element (antenna) above a ground screen loaded with a cell-dependent and frequency-dependent impedance $Z_{nm}(f)$, with $n = 0, 1, \ldots N-1$, $m = 0, 1, \ldots M-1$, and f being the frequency. The impedance is designed in such a way it is not matched to the antenna impedance Z_0, thus determining a reflected wave which is irradiated back by the radiation element. The corresponding frequency-dependent reflection coefficient in the presence of an incident plane wave with 3D angle $\Theta_{\text{inc}} = (\theta_{\text{inc}}, \phi_{\text{inc}})$ and observed at angle $\Theta = (\theta, \phi)$ is[1] [38], [39]

$$r_{nm}(\Theta_{\text{inc}}, \Theta; f) = \sqrt{F(\Theta_{\text{inc}}) \, F(\Theta)} \, G_{\text{c}} \, \Gamma_{nm}(f)$$
$$= \beta_{nm}(\Theta_{\text{inc}}, \Theta; f) \, e^{\jmath \, \Psi_{nm}(f)} \quad (1)$$

where $F(\Theta)$ is the normalized power radiation pattern that accounts for possible non-isotropic behavior of the radiation element, which we consider, as a first approximation, frequency-independent within the bandwidth of interest, G_{c} is the boresight antenna gain, $\Gamma_{nm}(f)$ is the frequency-dependent load reflection coefficient, $\beta_{nm}(\Theta_{\text{inc}}, \Theta; f)$ is the reflection amplitude and $\Psi_{nm}(f)$ is the reflection phase.[2] For instance, in [39] the following parametric shape for $F(\Theta)$ is proposed

$$F(\Theta) = \begin{cases} \cos^q(\theta) & \theta \in [0, \pi/2], \phi \in [0, 2\pi] \\ 0 & \text{otherwise} \end{cases} \quad (2)$$

Parameter q depends on the specific technology adopted as well as on the dimension of the cell and it is related to the boresight gain $G_{\text{c}} = 2(q+1)$. Following an approach similar to that in [39], one possibility is to set G_{c} so that the effective area

---

[1] We adopt the conventional spherical coordinate system where $\phi \in [0, 2\pi)$ (azimuth) and $\theta \in [0, \pi)$ (inclination).

[2] A more rigorous model should also account for the signal reflected back by the antenna according to its structural radar cross section (RCS) component [44].

of the cell is equal to the geometric area of the cell $A_{\text{c}} = d_x \, d_y$, i.e., $G_{\text{c}} = A_{\text{c}} \, 4\pi/\lambda^2$, assuming an ideal radiation efficiency. Considering a cell with $d_x = d_y = \lambda/2$, it follows that $G_{\text{c}} = \pi \simeq 5\,\text{dBi}$, and $q = 0.57$. A similar model is presented in [38] with $q = 3$. The load reflection coefficient is given by

$$\Gamma_{nm}(f) = \frac{Z_{nm}(f) - Z_0}{Z_{nm}(f) + Z_0} \,. \quad (3)$$

By properly designing the impedance $Z_{nm}(f)$ at each cell it is possible to realize different reflecting behaviors of the metasurface, as it will be investigated in this paper. Regardless of the specific technology adopted, we propose to design the reflection phase shift of the metasurface, $\Psi_{nm}(f)$. so that it exhibits a linear behavior with the frequency f, i.e.,

$$\Psi_{nm}(f) = \alpha_{nm} \cdot (f - f_{\text{r}}) + \gamma(f) \quad (4)$$

for f within the signal bandwidth W, where α_{nm} is a cell-dependent coefficient and $\gamma(f)$ is a (possibly present) frequency-dependent phase shift.[3] In particular, $\gamma(f)$ represents a common (among cells) phase offset which is irrelevant to beamsteering and focusing operations. For this reason in the remaining text we will neglect it. Note that α_{nm} refers to the nmth cell located at position $\mathbf{p}_{nm}$. According to the desired reflection behavior, as discussed in sections IV and V, the reference frequency f_{r} can be chosen either equal to the center frequency f_0 of the signal or equal to the lowest frequency edge of the signal band, i.e., $f_{\text{r}} = f_0 - W/2$. We will show that, thanks to the form in (4), it is possible to obtain a metasurface with the desired reflection properties allowing for frequency-dependent beamsteering and focusing; for this reason, we name it *metaprism*.

B. Design Example

We illustrate an example of how the phase response (4) can be approximated starting from the equivalent model in Fig. 2 described by (1), (2), and (3). To this purpose, we consider a purely reactive impedance $Z_{nm}(f) = \jmath X_{nm}(f)$ and a purely resistive antenna impedance $Z_0 = R_0$. The phase profile is

$$\Psi_{nm}(f) = \arg \Gamma_{nm}(f) = -2 \arctan \frac{X_{nm}(f)}{R_0} \,. \quad (5)$$

Suppose the reactive impedance consists of a resonating series LC circuit, with cell-dependent inductive and capacitive values L_{nm} [H] and C_{nm} [Farad], respectively. The corresponding impedance is

$$Z_{nm}(f) = \jmath X_{nm}(f) = -\jmath \frac{1 - (2\pi f)^2 L_{nm} C_{nm}}{2\pi f C_{nm}} \quad (6)$$

where L_{nm} and C_{nm} are chosen to satisfy $(2\pi\sqrt{L_{nm}C_{nm}})^{-1} = f_{\text{r}}$. To obtain the form in (4), it is convenient to derive the first-order Taylor series expansion in f for the reflection coefficient phase with respect to the reference frequency f_{r}. In particular, for the LC load it results

$$\Psi_{nm}(f) \simeq -\frac{8\pi L_{nm}}{R_0}(f - f_{\text{r}}) \,. \quad (7)$$

---

[3] From the practical point of view, the phase profile can be implemented equivalently according to a 2π modulo operation.

From (7) it is possible to obtain the desired coefficient $\alpha_{nm} = -8\pi L_{nm}/R_0$ in (4) by properly designing L_{nm} and C_{nm} in each cell. From the technological point of view, examples of metasurfaces whose elementary cells can be modeled as a purely reactive impedance can be found in [22], [43]. In particular, in [22] a cell made of a ring loaded square patch with a single varactor diode connected across the gap between the ring and the patch is proposed and modeled using both a full-wave solver and an equivalent LC circuit. In that paper, the frequency-selectivity of the cell is exploited to support the operation in two frequency bands.

C. Reflections from the Environment

A location in NLOS channel condition might still be covered even in the absence of a reflecting metasurface if a sufficient signal-to-noise ratio (SNR) is obtained from the signal scattered by the surrounding walls (e.g., buildings). Therefore, for a fair comparison between the performance achieved with and without metaprisms, it is important to consider also the signals scattered by walls. To this purpose, in this section we summarize the common models used to describe the scattering process in typical rough surfaces like walls. As a reference, we consider the scattering process modeled as the superimposition of a specular component obeying the Snell's law and a diffuse scattering component. The latter can be further modeled according to the widely-used Lambertian model [45], [46].

For convenience, we discretize the wall in the same way as the metaprism, i.e., with small areas A_c (cells) at positions $\mathbf{p}_{nm}$, with $n = 0, 1, \ldots N_w - 1$ and $m = 0, 1, \ldots M_w - 1$.[4] In the presence of an incident plane wave with angle Θ_{inc}, the Lambertian model at the observed angle Θ can be equivalently described in terms of the reflection coefficient of each cell as follows

$$r_{nm}(\Theta_{\text{inc}}, \Theta) = \Gamma(\theta_{\text{inc}}) \, R \sqrt{G_S} + S \sqrt{G_S \cos\theta_{\text{inc}} \, \cos\theta} \; e^{J\Psi_{nm}(\Theta_{\text{inc}}, \Theta)} \tag{8}$$

where $G_S = A_c \, 4\pi/\lambda^2$, $\Gamma(\theta_{\text{inc}})$ is the Fresnel reflection coefficient, R is the reflection reduction factor, and S is the scattering coefficient [46]. In (8) the first term corresponds to the specular component (since all cells have the same phase, the reflection results to be specular), whereas the second component refers to the Lambertian scattering pattern. When analyzing the scattering coefficient in direction Θ, the phase shift $\Psi_{nm}(\Theta_{\text{inc}}, \Theta)$ at position $\mathbf{p}_{nm}$ is determined so that the signals reflected by all the cells sum up coherently towards angle Θ, i.e.,

$$\Psi_{nm}(\Theta_{\text{inc}}, \Theta) = -\frac{2\pi \, n \, d_x}{\lambda} \left(u_x(\Theta_{\text{inc}}) + u_x(\Theta) \right)$$
$$-\frac{2\pi \, m d_y}{\lambda} \left(u_y(\Theta_{\text{inc}}) + u_y(\Theta) \right) + \Psi_0 \tag{9}$$

where Ψ_0 is a common phase offset and, for convenience, we have defined the quantities $u_x(\Theta) = \sin(\theta)\cos(\phi)$ and $u_y(\Theta) = \sin(\theta)\sin(\phi)$.

---

[4] N_w and M_w are in general larger than N and M as walls have typically a larger extension.

III. System Model

For further convenience, it is worth to define the Fraunhofer distance $d_{\text{Fraunhofer}} = 2 D^2/\lambda$ and the Fresnel distance $d_{\text{Fresnel}} = \sqrt[3]{D^4/8\lambda}$ [44], where $D = \max(L_x, L_y)$ is the surface's size. At distance $d > d_{\text{Fraunhofer}}$ between the surface and the transmit/receive antennas, the communication takes place in the far-field region and only beamsteering is possible because of the plane wave propagation. Instead, when $d < d_{\text{Fraunhofer}}$, the communication takes place in the near-field region[5] and focusing is possible due to the spherical wavefront propagation [17]. For instance, at $f_0 = 28\,\text{GHz}$ and with a surface of size $D = 0.5\,\text{m}$ it is $d_{\text{Fraunhofer}} = 50$ meters. It follows that when operating at millimeter waves or beyond, the far-field assumption becomes no longer valid also at practical distances of operation for relatively small antennas/surfaces. Therefore, design approaches based on this assumption should be revisited, as done in this paper.

A. Scenario Considered

We consider a downlink OFDM-based wireless system where a BS serves U single-antenna fixed users located in NLOS condition with respect to it, as illustrated in Fig. 1. In our study, we assume the BS is in LOS condition and in the far-field region with respect to the reflecting surface (metaprism or wall). Moreover, we consider all the users are located in LOS condition with respect to the surface but they could be in near- or far-field region depending on their distance from the surface, as it will be analyzed in the next sections. In a conventional OFDM system, the total bandwidth W is equally divided into $K \geq U$ orthogonal subcarriers with subcarrier spacing $\Delta f = W/K$. The frequency of the kth subcarrier is $f_k = f_0 - W/2 + k\Delta f$, $k = 1, 2, \ldots, K$, where f_0 denotes the central frequency. To each user u, with $u \in \{1, 2, \ldots U\}$, a specific subcarrier $k = A(u)$ is one-to-one assigned according to some policy, as it will be specified in Section VII, where $A(u)$ is the assignment function and $A^{-1}(k)$ is its inverse. The case where a user requires more subcarriers (higher traffic) can be easily managed by grouping different subcarriers into a single resource block. Given the user u, denote by $x^{(k)} \in C$, with $\mathbb{E}\left\{ |x^{(k)}|^2 \right\} = 1$ and $k = A(u)$, its information symbol transmitted at the generic OFDM frame, being $\mathbb{E}\{.\}$ the statistical expectation operator. The total transmitted power P_T is allocated differently among subcarriers (and hence users) by multiplying the corresponding transmitted symbols by the weights $\omega^{(k)}$, $k = 1, 2, \ldots, K$, which account for the relative power assigned to each subcarrier under the constraint $\sum_k \left(\omega^{(k)} \right)^2 = 1$. The optimization of the distribution of the weights will be addressed in Section VII.

Consider the transmitting BS located in position $\mathbf{p}_{\text{BS}}$ and whose transmitted signal impinges the metaprism at distance $|\mathbf{p}_{\text{BS}} - \mathbf{p}_0| = |\mathbf{p}_{\text{BS}}|$, and angle-of-arrival (AOA) $\Theta_{\text{inc}} = (\theta_{\text{inc}}, \phi_{\text{inc}})$, with respect to the normal direction of the metaprism. When the relative bandwidth satisfies $W/f_0 \ll 1$,

---

[5] Here we are considering the radiating near-field region. The reactive near-field component becomes significant at distances typically less than d_{Fresnel} [44].

the complex channel gain between the transmitter and the nmth cell of the metaprism for the kth subcarrier is

$$h_{nm}^{(k)}(\mathbf{p}_{\text{BS}}) = \frac{\sqrt{G_{\text{T}}}\lambda}{4\pi|\mathbf{p}_{\text{BS}} - \mathbf{p}_{nm}|} \exp\left(-J\frac{2\pi f_k}{c}|\mathbf{p}_{\text{BS}} - \mathbf{p}_{nm}|\right) \quad (10)$$

where G_{T} is the transmit antenna gain, and $\lambda = c/f_0$, with c being the speed of light. Similarly, the channel gain from the nmth cell to the receiver located in position $\mathbf{p} = (x, y, z)$ is

$$g_{nm}^{(k)}(\mathbf{p}) = \frac{\sqrt{G_{\text{R}}}\lambda}{4\pi|\mathbf{p} - \mathbf{p}_{nm}|} \exp\left(-J\frac{2\pi f_k}{c}|\mathbf{p} - \mathbf{p}_{nm}|\right) \quad (11)$$

where G_{R} is the receive antenna gain. By combining the previous expressions, the received signal at the kth subcarrier is given by

$$y^{(k)} = \sum_{n=0}^{N-1}\sum_{m=0}^{M-1} h_{nm}^{(k)}(\mathbf{p}_{\text{BS}})\, r_{nm}^{(k)}(\Theta_{\text{inc}}, \Theta)\, g_{nm}^{(k)}(\mathbf{p})\, \sqrt{P_{\text{T}}}\, \omega^{(k)} x^{(k)} + n^{(k)}$$

$$= \sqrt{P_{\text{T}}}\, c^{(k)}(\mathbf{p}_{\text{BS}}, \mathbf{p})\, \omega^{(k)}\, x^{(k)} + n^{(k)} \quad (12)$$

where $\Theta = (\theta, \phi)$ is the angle corresponding to position $\mathbf{p}$, $n^{(k)}$ is the thermal noise modeled as a zero-mean complex circular symmetric Gaussian random variable (RV) with variance σ_n^2, and $r_{nm}^{(k)}(\Theta_{\text{inc}}, \Theta) = r_{nm}(\Theta_{\text{inc}}, \Theta; f_k)$ is the surface's reflection coefficient at frequency f_k given by (1). The phase shift and gain undertaken by the kth subcarrier from the nmth cell are, respectively,

$$\Psi_{nm}^{(k)} = \Psi_{nm}(f_k)$$
$$\beta_{nm}^{(k)}(\Theta_{\text{inc}}, \Theta) = \beta_{nm}(\Theta_{\text{inc}}, \Theta; f_k). \quad (13)$$

It is worth to notice that the detection of $x^{(k)}$ requires only the estimation of the cascaded channel coefficient $c^{(k)}(\mathbf{p}_{\text{BS}}, \mathbf{p})$, i.e., the end-to-end estimation of the CSI, which includes the BS-metaprism and metaprism-user channels. A discussion on the advantages in CSI estimation brought by metaprisms with respect to RIS-based systems will be provided in Section VIII-D.

IV. Subcarrier-dependent Beamsteering

In this section, we investigate how, through a proper design of coefficients α_{nm} in (4) characterizing the cells of the metaprism, it is possible to perform subcarrier-dependent beamsteering when both the transmitter and the receiver are in the LOS far-field region with respect to the metaprism. First, for a given incident signal with angle Θ_{inc}, we find the relationship between the incident and reflection angles as a function of subcarrier k and the coefficients α_{nm}. Then we provide an example in which the metaprism is designed so that when f_k ranges from f_1 to f_K (the entire OFDM bandwidth), the corresponding reflected angles span within a given interval. This opens the possibility to control the reflection angle through proper subcarrier assignment to users instead of configuring in real-time the metasurface, as it will be explained in Section VII.

In far-field condition, equation (10) can be well approximated as (plane wavefront) [44]

$$h_{nm}^{(k)}(\mathbf{p}_{\text{BS}}) \simeq \frac{h_0}{|\mathbf{p}_{\text{BS}}|} \exp\left(J\frac{2\pi}{\lambda}\left(nd_x\, u_x(\Theta_{\text{inc}}) + md_y\, u_y(\Theta_{\text{inc}})\right)\right) \quad (14)$$

where $h_0 = \sqrt{G_{\text{T}}}\frac{\lambda}{4\pi}\exp\left(-J\frac{2\pi}{\lambda}|\mathbf{p}_{\text{BS}}|\right)$. The exponential argument accounts for the phase shift with respect to the metaprism center $\mathbf{p}_0$. Similarly, (11) can be approximated as

$$g_{nm}^{(k)}(\mathbf{p}) \simeq \frac{g_0}{|\mathbf{p}|} \exp\left(J\frac{2\pi}{\lambda}\left(nd_x\, u_x(\Theta) + md_y\, u_y(\Theta)\right)\right) \quad (15)$$

where $g_0 = \sqrt{G_{\text{R}}}\frac{\lambda}{4\pi}\exp\left(-J\frac{2\pi}{\lambda}|\mathbf{p}|\right)$. We consider the particular but significant case where $\beta_{nm}^{(k)}(\Theta_{\text{inc}}, \Theta) = \beta_0^{(k)}(\Theta_{\text{inc}}, \Theta)$, $\forall n, m$, so that using the approximations (14) and (15), equation (12) can be written as

$$y^{(k)} = \frac{\sqrt{P_{\text{T}}}\, h_0\, g_0\, \beta_0^{(k)}(\Theta_{\text{inc}}, \Theta)}{|\mathbf{p}_{\text{BS}}|\, |\mathbf{p}|}\, \omega^{(k)}\, x^{(k)} \quad (16)$$

$$\cdot \sum_{n=0}^{N-1}\sum_{m=0}^{M-1} \exp\left(J\frac{2\pi nd_x}{\lambda}\left(u_x(\Theta_{\text{inc}}) + u_x(\Theta)\right)\right.$$

$$\left. + J\frac{2\pi md_y}{\lambda}\left(u_y(\Theta_{\text{inc}}) + u_y(\Theta)\right) + J\Psi_{nm}^{(k)}\right) + n^{(k)}.$$

The phase profile the metaprism should obey, at frequency f_k, to have the signal components related to the kth subcarrier reflected towards a target direction $\Theta_0^{(k)} = \left(\theta_0^{(k)}, \phi_0^{(k)}\right)$, is

$$\Psi_{nm}^{(k)} = -\frac{2\pi nd_x}{\lambda}\left(u_x(\Theta_{\text{inc}}) + u_x\left(\Theta_0^{(k)}\right)\right)$$
$$- \frac{2\pi md_y}{\lambda}\left(u_y(\Theta_{\text{inc}}) + u_y\left(\Theta_0^{(k)}\right)\right) \quad (17)$$

so that all the phasors in (16) sum up coherently in the direction $\Theta_0^{(k)}$. Note that one could see the system transmitter-metaprism as an equivalent planar antenna array (reflectenna) whose frequency-dependent array factor is

$$AF^{(k)}(\Theta) = \sum_{n=0}^{N-1}\sum_{m=0}^{M-1} \exp\left(J\frac{2\pi nd_x}{\lambda}\left(u_x(\Theta) - u_x\left(\Theta_0^{(k)}\right)\right)\right.$$

$$\left. + J\frac{2\pi md_y}{\lambda}\left(u_y(\Theta) - u_y\left(\Theta_0^{(k)}\right)\right)\right) \quad (18)$$

having $\beta_0^{(k)}(\Theta_{\text{inc}}, \Theta)$ as pattern of each antenna element.

Now, with reference to (4), suppose we set $f_{\text{r}} = f_0$ and we design the cell-dependent coefficients α_{nm}, $n = 0, 1, \ldots, N$, $m = 0, 1, \ldots M - 1$, such as they are related to the cell's positions $\mathbf{p}_{nm} = (x_n, y_m)$ as follows

$$\alpha_{nm} = a_0\, x_n + b_0\, y_m \quad (19)$$

with a_0 and b_0 being two constants to be properly designed. The frequency-dependent phase profile results

$$\Psi_{nm}(f) = \alpha_{nm} \cdot (f - f_0) = (a_0\, x_n + b_0\, y_m) \cdot (f - f_0). \quad (20)$$

By equating (20) and (17) it is

$$a_0(f_k - f_0) = -\frac{2\pi}{\lambda}\left(u_x(\Theta_{\text{inc}}) + u_x\left(\Theta_0^{(k)}\right)\right)$$

$$b_0(f_k - f_0) = -\frac{2\pi}{\lambda}\left(u_y(\Theta_{\text{inc}}) + u_y\left(\Theta_0^{(k)}\right)\right) \quad (21)$$

Fig. 3. Normalized equivalent array factor for some values of the subcarrier index k. $N = M = 100$, $d_x = d_y = \lambda/2$. $\theta_{\text{inc}} = 45°$, $\phi_{\text{inc}} = 0°$, $\theta_m = 40°$.
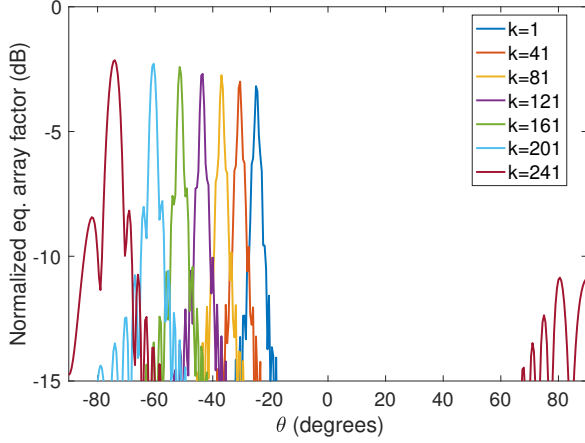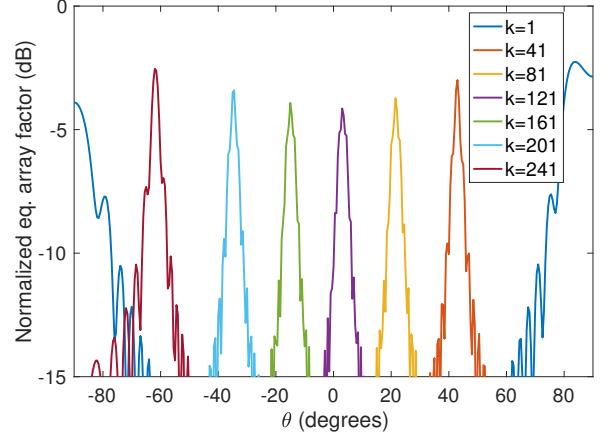

Fig. 4. Normalized equivalent array factor for some values of the subcarrier index k. $N = M = 100$, $d_x = d_y = \lambda/2$. $\theta_{\text{inc}} = 0°$, $\phi_{\text{inc}} = 0°$, $\theta_m = 90°$.

from which we can determine the reflection direction $\Theta_0^{(k)}$ as a function of the subcarrier k

$$u_x\left(\Theta_0^{(k)}\right) = -u_x(\Theta_{\text{inc}}) - \frac{a_0\,\lambda}{2\pi}(f_k - f_0)$$

$$u_y\left(\Theta_0^{(k)}\right) = -u_y(\Theta_{\text{inc}}) - \frac{b_0\,\lambda}{2\pi}(f_k - f_0)\,. \tag{22}$$

Equation (22) indicates that each subcarrier is reflected towards a different direction depending on the incident angle Θ_{inc}, the coefficients a_0 and b_0, and hence of cells' coefficients α_{nm} using (19). In the next section we provide a design example making use of (22).

A. Design Example

Suppose that the signal transmitted by the BS impinges the metaprism with incident angle $\Theta_{\text{inc}} = (\theta_{\text{inc}}, 0)$ in the $x - z$ plane[6] and that we want the metaprims reflects the signal so that the signal component related to subcarrier $k = K$ (the highest subcarrier) is reflected with angle $\theta_0^{(K)} = -\theta_{\text{inc}} - \theta_m$, $\phi_0^{(k)} = 0$, for some angle θ_m, and the other subcarriers are reflected with different increasing angles in order to span a specific NLOS area. Note that according to (22) for the central subcarrier $k_0 = K/2$, corresponding to $f_{k_0} = f_0$, it is $\theta_0^{(k_0)} = -\theta_{\text{inc}}$, independently of a_0 and b_0. From (21), by setting $k = K$, the design coefficients in (20) result

$$a_0 = -\frac{2\pi}{\lambda(f_K - f_0)}\left(u_x(\Theta_{\text{inc}}) + u_x\left(\Theta_0^{(K)}\right)\right)$$

$$= -\frac{4\pi}{\lambda W}\left(-\sin(\theta_{\text{inc}} + \theta_m) + \sin(\theta_{\text{inc}})\right)$$

$$b_0 = -\frac{2\pi}{\lambda(f_K - f_0)}\left(u_y(\Theta_{\text{inc}}) + u_y\left(\Theta_0^{(K)}\right)\right) = 0\,. \tag{23}$$

With this choice of a_0 and b_0, from (22) we obtain

$$\sin\left(\theta_0^{(k)}\right) = -\sin(\theta_{\text{inc}}) + \frac{2(f_k - f_0)}{W}\left(\sin(-\theta_{\text{inc}} - \theta_m) + \sin(\theta_{\text{inc}})\right)\,. \tag{24}$$

[6]To lighten the treatment, sometimes we take the liberty of derogating from the conventional spherical coordinate system by allowing θ ranging in $[-\pi/2, \pi/2)$ and $\phi \in [0, \pi)$.

The extreme case where $k = 1$ (the lowest subcarrier) gives $\sin\left(\theta_0^{(1)}\right) = -2\sin(\theta_{\text{inc}}) + \sin(\theta_{\text{inc}} + \theta_m)$. As result, each subcarrier is reflected according to a different angle in the range $\left[\theta_0^{(K)}, \theta_0^{(1)}\right]$, around the Snell's angle $-\theta_{\text{inc}}$, thus creating the "prism" behavior.

A numerical example is provided in Fig. 3, where the equivalent frequency-dependent array factor of the transmitter-metaprism given by (18), normalized with respect to $N \times M$, is shown for some subcarrier indexes as a function of the observation angle $\theta \in [-90°, +90°]$. Coefficients a_0 and b_0 have been computed using (23) with the following parameters: $\theta_{\text{inc}} = 45°$, $\phi_{\text{inc}} = 0°$, $\theta_m = 40°$, $\lambda W = 10^6$ and $K = 256$. It can be easily verified that the main lobe of the equivalent array factor shifts from $\theta_0^{(1)} \simeq -25°$ to $\theta_0^{(K)} = -\theta_{\text{inc}} - \theta_m = -85°$, when the subcarrier index ranges from 1 to K. Another example is given in Fig. 4 where $\theta_{\text{inc}} = 0°$, $\phi_{\text{inc}} = 0°$, $\theta_m = 90°$, corresponding to the coefficient $a_0 = -8\pi/\lambda W$. With this design, the main lobe of the equivalent array factor spans in the range $[-90°, +90°]$. In case the equivalent model for the metaprism is that introduced in Section II-B, by substituting a_0 in (7), we obtain directly the values of the load's inductance $L_{nm} = n\,R_0/(2\,W)\,[\text{H}]$ to be assigned to the cell at position $\mathbf{p}_{nm}$.

V. Subcarrier-dependent Focusing

Following a similar approach as in Section IV, we suppose now the receiver is in the near-field region with respect to the metaprism whereas the BS is still in far-field. Denoting with Θ_{inc} the incident angle of the signal, if one wants to focus the signal component associated to subcarrier k on position $\mathbf{p}$, with angle $\Theta_0^{(k)}$ and distance $d_F^{(k)} = |\mathbf{p}|$, all the components in (12) must sum up coherently in that position. Note that now in (12) the exact expression (11) should be used instead of (15). Considering the following approximation $|\mathbf{p} - \mathbf{p}_{nm}| \simeq |\mathbf{p}|$, which holds when the receiver is not too close to the metaprism (i.e., $d^{(k)} > d_{\text{Fresnel}}$), the coherent sum corresponds to designing the metaprism so that the phase profile for the

kth subcarrier results (Fresnel approximation) [17]

$$\Psi_{nm}^{(k)} = \frac{2\pi}{\lambda} \frac{(x_n^2 + y_m^2)}{2d_F^{(k)}} - \frac{2\pi x_n}{\lambda} \left(u_x(\Theta_{inc}) + u_x \left(\Theta_0^{(k)} \right) \right)$$
$$- \frac{2\pi y_m}{\lambda} \left(u_y(\Theta_{inc}) + u_y \left(\Theta_0^{(k)} \right) \right) . \tag{25}$$

It is convenient to choose $f_r = f_1$ in (4) so that $d_F^{(k)} > 0$, $\forall k$, and to design the cell-dependent coefficient α_{nm} with the following position-dependent expression

$$\alpha_{nm} = a_F \left(x_n^2 + y_m^2 \right) + a_0 x_n + b_0 y_m \tag{26}$$

with parameters a_F, a_0 and b_0 to be properly designed. From (4) and (25) it is

$$\Psi_{nm}^{(k)} = \alpha_{nm} \cdot (f_k - f_1)$$
$$= \left[a_F \left(x_n^2 + y_m^2 \right) + a_0 x_n + b_0 y_m \right] \cdot (f_k - f_1) \tag{27}$$

from which we can determine the focal distance obtained at each frequency

$$d_F^{(k)} = \frac{\pi f_1}{c \, a_F \, (f_k - f_1)} \tag{28}$$

as a function of parameter a_F, whereas a_0 and b_0 can be designed according to the criteria given in the previous section once the target direction $\Theta_0^{(k)}$ is fixed.

A. Design Example

For instance, parameter a_F can be designed so that, given a minimum desired focal distance d_m, it is $d_F^{(k)} = d_m$ when $k = K$, i.e., $a_F = \pi f_1/(c \, d_m \, W)$. When moving to lower subcarrier indexes the focal distance will increase to infinity (when $k = 1$). It is worth to notice that the phase profile in (27) degenerates to that of beamsteering in (17) (with f_1 instead of f_0) when approaching the far-field region, i.e., when $d_F^{(k)} \approx d_{Fraunhofer}$, or when entering the far-field region. This means that when increasing the focal distance it is no longer possible to discriminate distances but only angles. Focusing can be helpful when one is interested in discriminating users located at different distances but with similar angles, as happens in mono-dimensional scenarios such as along corridors or streets. An example will be presented in the numerical results.

VI. SOME CONSIDERATIONS ABOUT THE PATH-LOSS WHEN USING METASURFACES

To compute the link-budget using metaprisms and, in general, large metasurfaces such as RISs, it is important to understand how the total path-loss depends on system parameters, in particular on the dimensions and characteristics of the metasurface. This topic has received some attention in recent literature regarding RIS-enabled wireless networks [20], [38], [39], [47]. However, in many cases, the validity range of the models obtained are not properly investigated.

In general, for a given design of the metaprism, the path-loss for subcarrier k can be computed from (1) and (12)

$$L^{(k)} = \left| c^{(k)}(\mathbf{p}_{BS}, \mathbf{p}) \right|^{-2}$$
$$= \frac{(4\pi)^4}{\lambda^4 G_T G_R G_c^2 \, F(\Theta_{inc}) \, F(\Theta)} \tag{29}$$
$$\cdot \left| \sum_{n=0}^{N-1} \sum_{m=0}^{M-1} \frac{\Gamma_{nm}(f_k)}{|\mathbf{p}_{BS} - \mathbf{p}_{nm}| \, |\mathbf{p} - \mathbf{p}_{nm}|} \right.$$
$$\left. \cdot \exp \left(-J \frac{2\pi f_k}{c} \left(|\mathbf{p}_{BS} - \mathbf{p}_{nm}| - |\mathbf{p} - \mathbf{p}_{nm}| \right) \right) \right|^{-2} .$$

The path-loss can be minimized by properly designing the amplitude and phase profiles of $\Gamma_{nm}(f)$ under the constraint that $|\Gamma_{nm}(f)| \le 1$ since the metaprism is supposed to be locally passive.

In the particular but significant case where $|\Gamma_{nm}(f)| = 1$, $|\mathbf{p}_{BS} - \mathbf{p}_{nm}| \simeq |\mathbf{p}_{BS}|$, $|\mathbf{p} - \mathbf{p}_{nm}| \simeq |\mathbf{p}|$ (amplitude approximation, i.e., transmitter and receiver are not too close to the metaprism) and the phase profile $\Psi_{nm}^{(k)}$ of the metaprism is designed to perfectly compensate the phase distortion introduced by the channel, i.e.,

$$\Psi_{nm}^{(k)} = \frac{2\pi f_k}{c} \left(|\mathbf{p}_{BS} - \mathbf{p}_{nm}| + |\mathbf{p} - \mathbf{p}_{nm}| \right) \tag{30}$$

equation (29) simplifies to

$$L^{(k)} \simeq \frac{(4\pi)^4 |\mathbf{p}_{BS}|^2 \, |\mathbf{p}|^2}{\lambda^4 G_T G_R G_c^2 \, F(\Theta_{inc}) \, F(\Theta) \, (N \, M)^2} \tag{31}$$

which was obtained also by other authors [38], [39], [47] under far-field conditions for RISs. Actually, the path-loss in (31) is valid also in near-field conditions provided the perfect phase profile (30) is considered.

Equation (31) may give the false illusion that by augmenting the number $N \times M$ of cells of the metasurface, the path-loss could be reduced arbitrarily. Unfortunately, this is true only under certain conditions and one should be careful in extrapolating this result, as commented in the following 3 arguments.

(i) - If the phase profile of the metasurface has been designed to perform beamsteering (as in most of papers), (31) is accurate only in far-field, i.e., when $|\mathbf{p}|$ and $|\mathbf{p}_{BS}|$ approach or overcome $d_{Fraunhofer}$. When decreasing the distance, the actual path-loss could degrade with respect to that predicted by (31) if different phase profiles are used. This is evident in the examples shown in Figs. 5 and 6, related to two different dimensions of the metasurface, where the path-loss obtained using (29) with phase profiles (17) (beamsteering), (25) (focusing), and (30) (i.e., using (31)) as a function of receiver distance is reported. At short distances, (31) could lead to very optimistic predictions if the phase profile was designed using beamsteering, especially when large metasurfaces are deployed. More favorable path-loss values can be obtained if one considers the focusing phase profile (25). When approaching the Fresnel distance $d_{Fresnel} \simeq 50\,cm$, also focusing using (25) becomes inaccurate and one has to consider the exact phase profile in (30), but near-field reactive effects will also emerge which make the analysis impossible
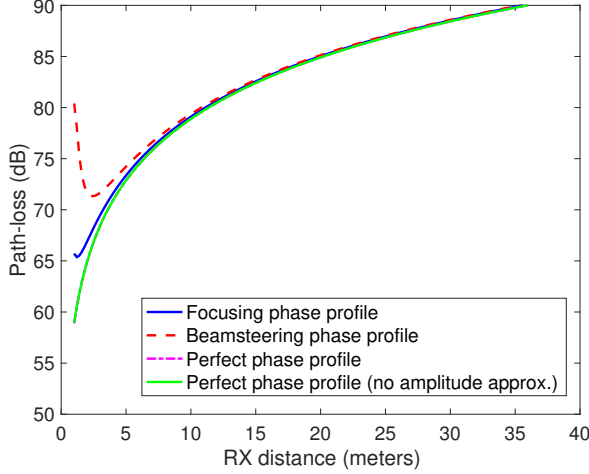
Fig. 5. Path-loss as a function of RX distance. TX located at 20 meters. Both TX and RX are located along the metaprism boresigth direction, $d_x = d_y = \lambda/2$, $f_0 = 28\,\text{GHz}$, $G_\text{T} = 10\,\text{dB}$, $G_\text{R} = 2\,\text{dB}$. $L_x = L_y = 25\,\text{cm}$.
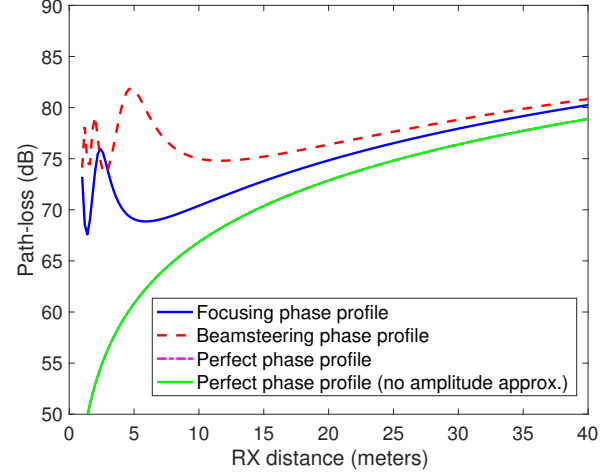

Fig. 6. Path-loss as a function of RX distance. TX located at 20 meters. Both TX and RX are located along the metaprism boresigth direction, $d_x = d_y = \lambda/2$, $f_0 = 28\,\text{GHz}$, $G_\text{T} = 10\,\text{dB}$, $G_\text{R} = 2\,\text{dB}$. $L_x = L_y = 50\,\text{cm}$.

without resorting to dedicated modeling at EM level. From Fig. 6, it is also evident that the amplitude approximation is in general accurate even at very short distances (magenta and green curves are almost overlapped).

(ii) - Expression (31), but also the general expression (29), assumes implicitly that the whole metasurface is illuminated by the transmitted signal (for reciprocity, the same arguments hold also for the receiver). This could not be true because of shadowing caused by the obstacle (for instance, in Fig. 1 if one extended the metasurface towards the NLOS area, part of the metasurface would not be illuminated by the BS). Even in LOS condition, only part of the metasurface would be illuminated if the transmitter (receiver) was close to the metasurface and/or its antenna had a large gain. In fact, the higher is the antenna gain, the narrower is the illuminating beam.

(iii) - In the presence of a large metasurface in relation to the distance, polarization mismatch could play an important role. Even if the transmit/receive antenna and cell elements are designed and deployed with the same polarization (e.g., vertical), when one of the antennas is located at a distance of the same order of magnitude as the metasurface's size, the cells at the edge of the metasurface might not be aligned with the impinging wave, thus generating a polarization mismatch which is not accounted for by (29). A detailed analysis of the path-loss and the coupling modes when using LIS antennas can be found in [19].

Before moving to the next section, it may be interesting to observe that when $\Theta_\text{inc} = \Theta = (0,0)$, (31) is nothing else than the radar equation in case of a perfect metal square plate with area $A = L_x \cdot L_y$, whose RCS at its boresight is $\rho_\text{m} = 4\pi A^2/\lambda^2$. In fact, it is $G_\text{c}{}^2 F(\Theta_\text{inc}) F(\Theta) (NM)^2 = (d_x d_y)^2 (NM)^2 (4\pi)^2/\lambda^4 = A^2 (4\pi)^2/\lambda^4 = \rho_\text{m} 4\pi/\lambda^2$, which inserted in (31) gives the well-known radar equation [44]. At different angles, the equivalent directional RCS of the metaprism is $\rho(\Theta_\text{inc}, \Theta) = 4\pi A^2 F(\Theta_\text{inc}) F(\Theta)/\lambda^2$ (assuming the perfect phase profile (30)), where the radiation pattern $F(\Theta)$ accounts also for the fact that the effective area of

the metaprism reduces when illuminated/observed at different angles. Summarizing, with an ideal design of the phase profile, the metaprism acts approximatively as a perfect metal plate reflecting at the location of interest, while with a different design one has to be careful when using (31).

VII. ACHIEVABLE RATE IN NLOS CONDITIONS

We investigate, in terms of achievable rate, the impact at the network level of using a metaprism to extend the coverage in NLOS areas. Specifically, we consider the network shown in Fig. 1, where U users are served by one BS. The achievable data rate (bit/s/Hz) at user u is given by

$$R_u = \log_2(1 + \text{SNR}_u) \tag{32}$$

where from (12)

$$\text{SNR}_u = P_\text{T} \left| c^{(A(u))}(\mathbf{p}_\text{BS}, \mathbf{p}_u)\, \omega^{(A(u))} \right|^2 / \sigma_n^2 \tag{33}$$

being $A(u)$ the subcarrier index assigned to user u, and $\mathbf{p}_u$ the position of user u. We assume the cascaded channel coefficient $c^{(A(u))}(\mathbf{p}_\text{BS}, \mathbf{p}_u)$ is perfectly estimated at the receiver (perfect end-to-end CSI). For instance, to obtain the CSI, during the initial access each user, in turn, could transmit a series of pilot symbols on all the subcarriers and the BS estimate the corresponding SNRs. Denote with $\text{SNR}(u, k)$, $u = 1, 2, \ldots U$, $k = 1, 2, \ldots K$, the SNR measured by the BS on subcarrier k when user u was accessing. This procedure should be repeated periodically to manage time variations of the channel conditions caused by propagation effects and/or movement of users. Once the end-to-end CSI has been estimated, the problem is how to assign subcarriers to the U users and how to determine the weights $\omega^{(k)}$, $k = 1, 2, \ldots K$, such that the per-user or network achievable rate is maximized.

The general optimization appears prohibitive from the complexity point of view and it is out of the scope of this paper. To obtain numerical results, we consider the sub-optimal assignment Algorithm 1. The aim of the algorithm is to

Algorithm 1: Subcarrier and weights assignment.

Input: Number of users U, SNR matrix $SNR(u, k)$
Result: Subcarriers assignment $\{A(u)\}$ and weights $\{\omega(k)\}$
$u = U$, $\omega(:) = 1/\sqrt{K}$;
while $u > 0$ **do**
   $[msnr, iu, ik] = max(SNR(u, k))$;   // search the couple user-subcarrier (iu, ik) experiencing the max SNR $msnr$
   if $u==U$ **then**
      $refsnr = msnr$;   // use the absolute max SNR as reference
   end
   $A(iu) = ik$; // assign subcarrier ik to user iu
   $SNR(iu, :) = 0$; // no longer consider user iu and subcarrier ik in the next steps
   $SNR(:, ik) = 0$;   //
   $\omega(ik) = \sqrt{refsnr/msnr}$; // compute the weights to equalize all the SNRs
   $u=u-1$;
end
$s = \sqrt{sum(\omega^2(k))}$;   // normalize the weights so that the sum of squares is one
for $u=1:U$ **do**
   $\omega(A(u)) = \omega(A(u))/s$;
end

Fig. 7. SNR map due to scattering from the wall (absence of metaprism). Aerial concrete wall with illuminated area of $4\,\mathrm{m}^2$.

guarantee all the users experience the same achievable rate. This is obtained by assigning subcarriers and weights $\omega^{(k)}$ to the users according to the estimated SNR at each subcarrier and user, i.e., the matrix $\mathrm{SNR}(u, k)$. The assignment is done in a greedy way starting from the couple user-subcarrier (u, k) experiencing the highest SNR. In the subsequent step, the couple user-subcarrier with the second-highest SNR, with the exclusion of the previously assigned user and subcarrier, is considered and so on. Details can be found in Algorithm 1. Such an assignment policy can be useful in those scenarios with a large number of users with common requirements in terms of achievable rate. An example is given by ultra-dense networks of sensors in industrial Internet of things (IoT) scenarios. Other optimization strategies are possible depending on application requirements, which can be the topic of future works.

VIII. NUMERICAL RESULTS

A. Scenario Considered

In the following, we corroborate the proposed metaprism idea with some numerical examples. The scenario considered is that illustrated in Fig. 1, where a transmitting BS is located at position $\mathbf{p}_{\mathrm{BS}} = (35.3, h, 35.3)$ meters, corresponding to a distance $d = 50$ meters from the metaprism and angle $\Theta_{\mathrm{inc}} = (45°, 0)$. We suppose the BS, the metaprism and the users are approximatively at the same height so that, without loss of generality, we set $h = 0$. If not otherwise specified, the following parameters have been used for the transmitter and the receiver: $f_0 = 28\,\mathrm{GHz}$ ($\lambda \simeq 1\,\mathrm{cm}$), $W = 100\,\mathrm{MHz}$, $K = 256$, $\Delta f = 390\,\mathrm{KHz}$, $P_{\mathrm{T}} = 8\,\mathrm{dBm}$, $G_{\mathrm{T}} = 6\,\mathrm{dB}$, $G_{\mathrm{R}} = 2\,\mathrm{dB}$, receiver noise figure $F = 3\,\mathrm{dB}$. The metaprism is composed of $N{\times}M$ elements with spacing $d_x = d_y = \lambda/2$. For what the wall
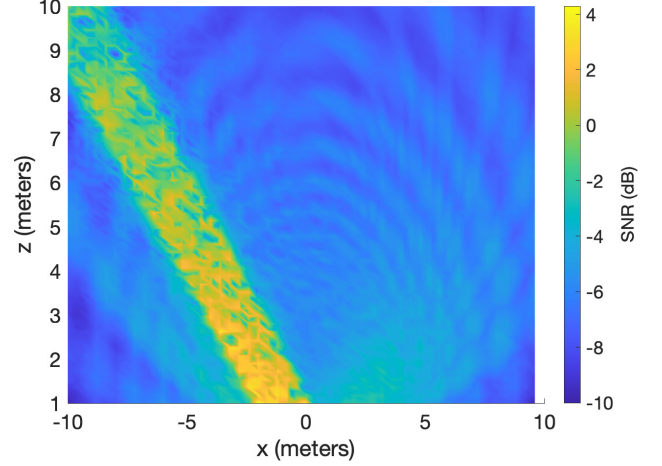
is regarded, it is supposed to be composed of areated concrete with EM parameters $\epsilon_r = 2.26$ (relative dielectric constant), $\tan\delta = 0.0491$ (loss tangent) [48], and scattering parameters $S^2 = 0.1$ (scattering coefficient), $R^2 = 0.9$ (reduction factor) [49]. All the locations on the left side of the scenario are in NLOS conditions because the signal from the BS is obstructed by the upper-side building. As a consequence, the only possibility users located in that area have to communicate with the BS is through specular/diffuse scattering from the wall and/or through the metaprism, when present.

B. SNR Maps

In Fig. 7, the SNR map obtained computing (33), with uniform power allocation among subcarriers, in a dense grid of locations in the absence of metaprism is shown. The presence of the specular component caused by the wall oriented towards the direction $\Theta = (-45°, 0)$, i.e., obeying the Snell's law, is evident. In practice, only the users located along this direction might have some chances for establishing a communication with the BS. The diffuse scattering component can in principle be exploited for communication as well, even though the corresponding SNR values are in general low.

The impact of the metaprism on the SNR map can be appreciated in Fig. 8. The phase profile of the metaprism has been designed according to the criterium illustrated in Section IV-A (beamsteering) by setting $\theta_m = 40°$ (note that $\theta_{\mathrm{inc}} = 45°$). The map is shown for some values of subcarrier index k, as indicated. The frequency-selective behavior of the metaprism allows to cover a wide range of angles in $\left[\theta_0^{(1)} = -25°, \theta_0^{(K)} = -85°\right]$, leading to the "prism effect". This effect can be exploited by the BS by assigning to the generic user located at angle θ_0 the subcarrier at which the metaprism reflects the signal towards θ_0. The corresponding SNR values are in general much higher than that obtained by exploiting only the reflections from the wall (compare with Fig. 7).

In Fig. 9, the SNR map is shown when the criterium in Section V (focusing) is used to design the phase profile of the metaprism by fixing the minimum focal distance $d_m =$
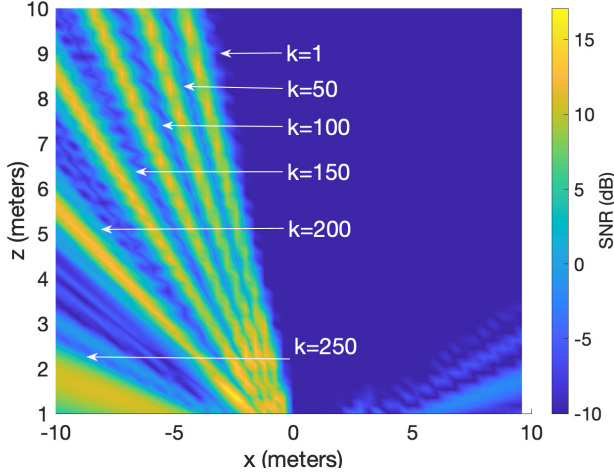
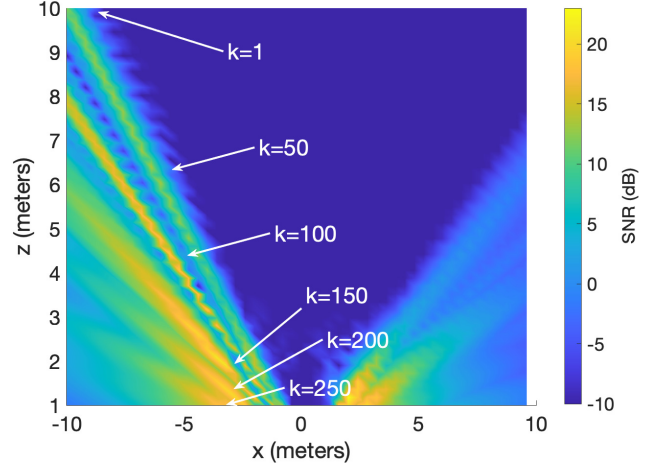Fig. 8. SNR map with the metaprism. Beamsteering phase profile. $L_x = L_y = 50\,\text{cm}$, $\theta_m = 40°$.

Fig. 9. SNR map with the metaprism. Focusing phase profile. $L_x = L_y = 50\,\text{cm}$. $d_m = 2\,\text{meters}$, $\theta_m = 5°$.

2 meters, and $\theta_m = 5°$. The map is shown for some values of subcarrier index k. Differently from Fig. 8, here it is evident that for each subcarrier the signal is more concentrated at a specific location (focal distance), especially when it is close to the metaprism. When moving from $k = K$ down to $k = 1$, the focusing distance increases from d_m to very large values, thus degenerating in beamsteering.

C. Achievable Rate

We now investigate the impact of the metaprism in terms of achievable rate (32) supposing U users are randomly located in the NLOS square area $x \in [-15, -5]$ meters, $z \in [2, 10]$ meters. The subcarrier assignment algorithm described in Section VII is used. The plots in Fig. 10 refer to the per-user achievable rate as a function of the number U of total users when different metaprism's sizes $L_x = L_y = L$ are considered. In the absence of the metaprism, L represents the dimension of the wall involved in the reflection, which depends in general on the geometry (e.g., presence of shadowed areas), and the directivity of the TX antenna. As expected, when increasing the size of the metaprism the achievable rate increases thanks to the more favorable path-loss. In the absence of metaprism (wall), only a small percentage of users fall within the small area corresponding to the specular reflection from the wall (at angle $\theta_0 = -45°$) or where the diffuse component is significant (see Fig. 7), and hence most of the users experience a bad SNR condition. Therefore, when increasing the number of users, the total available transmitted power is no longer sufficient to guarantee the same achievable rate to all the users at a significant level. A way out is to change the allocation policy by satisfying only a few users in good SNR condition and discarding all the others. In any case, the coverage of the system is in general poor. On the contrary, when the metaprism is introduced, the performance improvement is very significant, at least a factor 5 with respect to its absence (only wall), even using metaprisms with practical dimension (e.g., $L = 50\,\text{cm}$). The decreasing behavior of the plots is due to the fact that when increasing the number of users the total

transmitted power is shared among more users included those experiencing bad SNR conditions that require more power (higher weight $\omega^{(k)}$) to counteract their SNR penalty (the policy in Section VII imposes all the users have the same achievable rate). Beyond a certain value of U, depending on the size of the metaprism, the per-user achievable rate drops to zero because the users in bad SNR condition drain all the available power, and hence it is no longer possible to guarantee the same achievable rate at a reasonable level. As before, by discarding these disadvantaged users, one can maintain high values of achievable rate for the other users. In any case, the coverage obtained using the metaprism is significantly increased, as it can be also deduced from the SNR map in Fig. 8.

When moving from a metaprism with dimension $L = 50\,\text{cm}$ to a metaprism with dimension $L = 100\,\text{cm}$, an interesting phenomenon can be observed. First, there is a slight decrease in the achievable rate and the curve dropping happens at lower values of U. This can be ascribed to the fact that by increasing the dimension of the metaprism, the corresponding equivalent array factor becomes more and more angle-selective. Then, the main lobes of the equivalent array factor related to two adjacent subcarriers tend to be less overlapped thus creating an angle gap between them that is not covered by the metaprism. All the users with angles falling in these gaps experience low SNR values. This problem can be overcome by increasing the number K of subcarriers or decreasing the total bandwidth W. Again, different subcarrier assignment policies would bring to different behaviors.

The achievable rate in case a RIS is used instead of a metaprism is reported in Fig. 10 for comparison. Making a fair comparison is not easy because the RIS can be configured to reflect only in a particular direction so that only one user per time can be served but with all the subcarriers available. Serving another user in a different position requires the reconfiguration of the RIS according to some time-division multiple access (TDMA) scheme. Therefore, for a fixed number U of users, the achievable rate reported for RIS in Fig. 10 has been
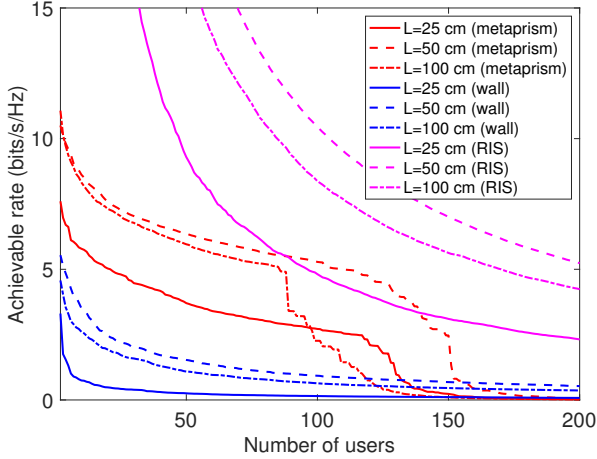
Fig. 10. Per-user achievable rate vs number of users for different surface's sizes.

Fig. 11. Per-user achievable rate vs number of users for different surface's sizes. Mono-dimensional scenario.

computed as $AR = AR_u/U$, where AR_u is the achievable rate when the RIS reflects towards user u, to account for the fact that U time slots are required to serve U users whereas only one time slot is needed in metaprism-based networks. We have neglected the time spent to control the RIS and required by the RIS to reconfigure itself, which represent critical issues in RISs and make the comparison not completely fair. Results show that with a perfect RIS, programmed to reflect exactly towards the desired user, significantly higher achievable rates are obtained. A more detailed discussion of the differences between RIS and metaprisms is provided in the next section.

Finally, we analyze the performance of focusing strategies when applied to a mono-dimensional scenario. In particular, we suppose the BS is located at 50 meters from the metaprism with angle $\theta_{\text{inc}} = 0°$, where U users are deployed randomly along the boresight direction of the metaprism in the range $[2, 10]$ meters. The beamsteering and focusing phase profiles in Sections IV-A and V, respectively, are compared in terms of achievable rate using the same subcarrier assignment algorithm. The following parameters have been used during the design: $d_m = 2$ meters, $\theta_m = 0°$. From the plots in Fig. 11, it can be observed that by designing the metaprism to perform focusing there is a valuable performance improvement of 30-50% with respect to a design based on beamsteering. The motivation is that, within the considered range, users are located in the near-field region, and hence they experience a path-loss advantage because of better signal concentration on user position (see Fig. 6) if the metaprism is designed to realize focusing, as discussed in Section VI.

D. Discussion on the Advantages and Disadvantages of Metaprisms

The metaprism concept proposed and investigated in this paper has to be considered as an alternative to conventional RIS. In this section, we discuss some practical implications of metaprism-based wireless networks compared to conventional RISs in order to understand when metaprisms may represent a better solution than RISs and when not.
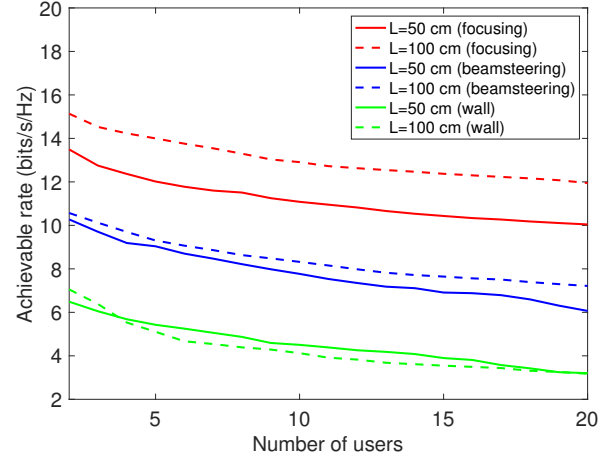
Unlike RISs, metaprisms are full passive (no energy supply needed) and they do not require a dedicated control channel to change their reflection properties, thus making them very appealing in all those situations where low cost, ease of deployment, and back compatibility with existing radio interfaces are required when extending the coverage of NLOS areas. Specifically, since with metaprisms the components of the transmitted signal related to a given subcarrier will always be reflected towards a given direction, the management of multiple users is delegated to the subcarrier assignment algorithm of the BS. Every change in the network (e.g., users' movement), requires a re-scheduling of subcarriers assignment to users. This does not represent, in general, an issue as subcarriers scheduling is a functionality already included in current standards such as LTE. However, such a fixed frequency-dependent reflection property prevents the assignment of a large number of subcarriers to the same user thus inhibiting a very high per-user data rate when only one or few users are present in the area.

On the contrary, in RIS-enabled networks, the metasurface must be configured every time a link has to be established with a particular user. This requires the estimation of the CSI involving a large number of channel coefficients. To this purpose, long pilot sequences have to be sent whose length is proportional to the number of elements composing the RIS (typically thousands) [33], [35], [36]. During the transmission of the pilot sequence, a dedicated control channel and protocol between the BS and the RIS must ensure that the RIS dynamically changes its coefficients according to pre-defined patterns [35]. Instead, with metaprims only one channel coefficient (per subcarrier) has to be estimated independently of the number of RIS's elements and no reconfiguration is necessary. In the presence of multiple users, the RIS has to be re-configured in order to reflect towards the intended user according to some TDMA scheme. One advantage of this way of operation is that, in principle, all the subcarriers can be assigned each time to the served user thus allowing higher per-user peak data rate, as evident in Fig. 10, but also higher latency because

of the TDMA scheduling. Therefore, metaprisms are better suited for dense networks with severe coverage issues (e.g., several NLOS areas), where a very large number of devices must be served in parallel with granted low-data rate and low-latency, which is a typical situation in industrial IoT scenarios. On the other hand, RIS-based networks are better suited for scenarios characterized by a few high-data rate users with less demanding latency constraints.

IX. CONCLUSION

In this paper, we have put forth the idea of *metaprism*, a full passive non-reconfigurable metasurface designed with a frequency-dependent phase profile such that its reflection properties are dependent on the subcarrier index when illuminated by an OFDM-like signal. We have provided design criteria for the phase profile of the metaprism to obtain subcarrier-dependent beamsteering and focusing functionalities. In addition, we have proposed an example of a low-complexity subcarrier assignment algorithm capable of guaranteeing all the users the same achievable rate. The numerical results have put in evidence the significant improvement, in terms of coverage and achievable rate, which can be obtained using metaprisms, with respect to the situation where radio coverage is delegated to the natural specular and diffuse reflection from walls. In particular, the examples provided show an achievable rate increase of a factor of 5 and more, even using relative small-size metaprisms (50 cm). We have also pointed out that, when operating at high frequencies (e.g., millimeter waves and beyond), the near-field region of the EM field is likely to extend to dozens of meters away from the metaprism, making the classical beamsteering-based design less efficient than the focusing-based design. Although metaprisms may not lead to the same achievable rate as RISs, the fact that they are full passive and allow parallel links pointing to different directions, makes them an appealing solution, especially in ultra-dense and low-latency industrial IoT scenarios. Future works will be devoted to the investigation of more complex networks including several BSs to evaluate the advantages of metaprisms in terms of interference reduction. Another area of research is related to the design of metasurfaces technologies tailored to the frequency-dependent characteristics introduced in this paper.

REFERENCES

[1] Z. Zhang, Y. Xiao, Z. Ma, M. Xiao, Z. Ding, X. Lei, G. K. Karagiannidis, and P. Fan, "6G wireless networks: Vision, requirements, architecture, and key technologies," *IEEE Vehicular Technology Magazine*, vol. 14, no. 3, pp. 28–41, Sep. 2019.

[2] T. S. Rappaport, Y. Xing, O. Kanhere, S. Ju, A. Madanayake, S. Mandal, A. Alkhateeb, and G. C. Trichopoulos, "Wireless communications and applications above 100 GHz: Opportunities and challenges for 6G and beyond," *IEEE Access*, vol. 7, pp. 78 729–78 757, 2019.

[3] T. S. Rappaport, Y. Xing, G. R. MacCartney, A. F. Molisch, E. Mellios, and J. Zhang, "Overview of millimeter wave communications for fifth-generation (5G) wireless networks: With a focus on propagation models," *IEEE Transactions on Antennas and Propagation*, vol. 65, no. 12, pp. 6213–6230, Dec 2017.

[4] E. Björnson, L. Sanguinetti, H. Wymeersch, J. Hoydis, and T. L. Marzetta, "Massive MIMO is a reality - what is next?: Five promising research directions for antenna arrays," *Digital Signal Processing*, 2019. [Online]. Available: http://www.sciencedirect.com/science/article/pii/S1051200419300776

[5] C. L. Holloway, E. F. Kuester, J. A. Gordon, J. O'Hara, J. Booth, and D. R. Smith, "An overview of the theory and applications of metasurfaces: The two-dimensional equivalents of metamaterials," *IEEE Antennas and Propagation Magazine*, vol. 54, no. 2, pp. 10–35, April 2012.

[6] S. B. Glybovski, S. A. Tretyakov, P. A. Belov, Y. S. Kivshar, and C. R. Simovski, "Metasurfaces: From microwaves to visible," *Physics Reports*, vol. 634, pp. 1 – 72, 2016. [Online]. Available: http://www.sciencedirect.com/science/article/pii/S0370157316300618

[7] I. A. Buriak, V. O. Zhurba, G. S. Vorobjov, V. R. Kulizhko, O. K. Kononov, and O. Rybalko, "Metamaterials: Theory, classification and application strategies (review)," *Journal of Nano- and Electronic Physics*, vol. 8, no. 4, 2016. [Online]. Available: https://search.proquest.com/docview/1853386963?accountid=9652

[8] D. Gonzlez-Ovejero, G. Minatti, G. Chattopadhyay, and S. Maci, "Multi-beam by metasurface antennas," *IEEE Transactions on Antennas and Propagation*, vol. 65, no. 6, pp. 2923–2930, 2017.

[9] L. Di Palma, A. Clemente, L. Dussopt, R. Sauleau, P. Potier, and P. Pouliguen, "Circularly-polarized reconfigurable transmitarray in Ka-band with beam scanning and polarization switching capabilities," *IEEE Transactions on Antennas and Propagation*, vol. 65, no. 2, pp. 529–540, Feb 2017.

[10] Y. Ra'di, V. S. Asadchy, and S. A. Tretyakov, "Tailoring reflections from thin composite metamirrors," *IEEE Transactions on Antennas and Propagation*, vol. 62, no. 7, pp. 3749–3760, July 2014.

[11] V. S. Asadchy, M. Albooyeh, S. N. Tcvetkova, A. Díaz-Rubio, Y. Ra'di, and S. A. Tretyakov, "Perfect control of reflection and refraction using spatially dispersive metasurfaces," *Phys. Rev. B*, vol. 94, p. 075142, Aug 2016. [Online]. Available: https://link.aps.org/doi/10.1103/PhysRevB.94.075142

[12] V. S. Asadchy, Y. Ra'di, J. Vehmas, and S. A. Tretyakov, "Functional metamirrors using bianisotropic elements," *Phys. Rev. Lett.*, vol. 114, p. 095503, Mar 2015. [Online]. Available: https://link.aps.org/doi/10.1103/PhysRevLett.114.095503

[13] S. V. Hum and J. Perruisseau-Carrier, "Reconfigurable reflectarrays and array lenses for dynamic antenna beam control: A review," *IEEE Transactions on Antennas and Propagation*, vol. 62, no. 1, pp. 183–198, Jan 2014.

[14] P. Nayeri, F. Yang, and A. Z. Elsherbeni, "Beam-scanning reflectarray antennas: A technical overview and state of the art." *IEEE Antennas and Propagation Magazine*, vol. 57, no. 4, pp. 32–47, Aug 2015.

[15] J. Hunt, J. Gollub, T. Driscoll, G. Lipworth, A. Mrozack, M. S. Reynolds, D. J. Brady, and D. R. Smith, "Metamaterial microwave holographic imaging system," *J. Opt. Soc. Am. A*, vol. 31, no. 10, pp. 2109–2119, Oct 2014. [Online]. Available: http://josaa.osa.org/abstract.cfm?URI=josaa-31-10-2109

[16] S. Hu, F. Rusek, and O. Edfors, "Beyond massive MIMO: The potential of data transmission with large intelligent surfaces," *IEEE Transactions on Signal Processing*, vol. 66, no. 10, pp. 2746–2758, May 2018.

[17] P. Nepa and A. Buffi, "Near-field-focused microwave antennas: Near-field shaping and implementation." *IEEE Antennas and Propagation Magazine*, vol. 59, no. 3, pp. 42–53, June 2017.

[18] N. Shlezinger, O. Dicker, Y. C. Eldar, I. Yoo, M. F. Imani, and D. R. Smith, "Dynamic metasurface antennas for uplink massive MIMO systems," *IEEE Transactions on Communications*, vol. 67, no. 10, pp. 6829–6843, 2019.

[19] D. Dardari, "Communicating with large intelligent surfaces: Fundamental limits and models," *IEEE Journal on Selected Areas in Communications*, vol. 38, no. 11, pp. 2526–2537, Nov 2020.

[20] E. Björnson and L. Sanguinetti, "Power Scaling Laws and Near-Field Behaviors of Massive MIMO and Intelligent Reflecting Surfaces," *arXiv e-prints*, p. arXiv:2002.04960, Feb. 2020.

[21] F. Guidi and D. Dardari, "Radio Positioning with EM Processing of the Spherical Wavefront," *IEEE Trans. on Wireless Comm.*, 2021, in publication.

[22] A. Tayebi, J. Tang, P. R. Paladhi, L. Udpa, S. S. Udpa, and E. J. Rothwell, "Dynamic beam shaping using a dual-band electronically tunable reflectarray antenna," *IEEE Transactions on Antennas and Propagation*, vol. 63, no. 10, pp. 4534–4539, Oct 2015.

[23] J. P. Turpin, J. A. Bossard, K. L. Morgan, D. H. Werner, and P. L. Werner, "Reconfigurable and tunable metamaterials: A review of the theory and applications," *International Journal of*

Antennas and Propagation, vol. 2014, 2014. [Online]. Available: https://doi.org/10.1155/2014/429837.

[24] C. Liaskos, A. Tsioliaridou, A. Pitsillides, S. Ioannidis, and I. Akyildiz, "Using any Surface to Realize a New Paradigm for Wireless Communications," *Communications of the ACM*, vol. 61, no. 11, pp. 30–33, 2018.

[25] C. Liaskos, S. Nie, A. Tsioliaridou, A. Pitsillides, S. Ioannidis, and I. Akyildiz, "A new wireless communication paradigm through software-controlled metasurfaces," *IEEE Communications Magazine*, vol. 56, no. 9, pp. 162–169, Sep. 2018.

[26] M. D. Renzo, M. Debbah, D.-T. Phan-Huy, A. Zappone, M.-S. Alouini, C. Yuen, V. Sciancalepore, G. C. Alexandropoulos, J. Hoydis, H. Gacanin, J. d. Rosny, A. Bounceur, G. Lerosey, and M. Fink, "Smart radio environments empowered by reconfigurable AI meta-surfaces: an idea whose time has come," *EURASIP Journal on Wireless Communications and Networking*, vol. 2019, no. 1, p. 129, 2019. [Online]. Available: https://doi.org/10.1186/s13638-019-1438-9

[27] Y. Yang, S. Zhang, and R. Zhang, "IRS-enhanced OFDM: Power allocation and passive array optimization," in *2019 IEEE Global Communications Conference (GLOBECOM)*, 2019, pp. 1–6.

[28] Ö. Özdogan, E. Björnson, and E. G. Larsson, "Using intelligent reflecting surfaces for rank improvement in MIMO communications," in *2020 IEEE International Conference on Acoustics, Speech and Signal Processing (ICASSP)*, 2020, pp. 9160–9164.

[29] M. Di Renzo, K. Ntontin, J. Song, F. H. Danufane, X. Qian, F. Lazarakis, J. De Rosny, D. T. Phan-Huy, O. Simeone, R. Zhang, M. Debbah, G. Lerosey, M. Fink, S. Tretyakov, and S. Shamai, "Reconfigurable intelligent surfaces vs. relaying: Differences, similarities, and performance comparison," *IEEE Open Journal of the Communications Society*, vol. 1, pp. 798–807, 2020.

[30] J. Ye, S. Guo, and M. S. Alouini, "Joint reflecting and precoding designs for SER minimization in reconfigurable intelligent surfaces assisted MIMO systems," *IEEE Trans. on Wireless Communications*, vol. 19, no. 8, pp. 5561–5574, 2020.

[31] S. Zhang and R. Zhang, "Capacity characterization for intelligent reflecting surface aided MIMO communication," *IEEE Journal on Selected Areas in Communications*, vol. 38, no. 8, pp. 1823–1838, 2020.

[32] M. Jung, W. Saad, M. Debbah, and C. S. Hong, "On the Optimality of Reconfigurable Intelligent Surfaces (RISs): Passive Beamforming, Modulation, and Resource Allocation," *arXiv e-prints*, p. arXiv:1910.00968, Oct 2019.

[33] Q. Wu, S. Zhang, B. Zheng, C. You, and R. Zhang, "Intelligent Reflecting Surface Aided Wireless Communications: A Tutorial," *arXiv e-prints*, p. arXiv:2007.02759, Jul. 2020.

[34] M. D. Renzo, A. Zappone, M. Debbah, M.-S. Alouini, C. Yuen, J. de Rosny, and S. Tretyakov, "Smart radio environments empowered by reconfigurable intelligent surfaces: How it works, state of research, and road ahead," *IEEE Journal Selected Areas in Communications*, 2020.

[35] C. You, B. Zheng, and R. Zhang, "Intelligent reflecting surface with discrete phase shifts: Channel estimation and passive beamforming," in *ICC 2020 - 2020 IEEE International Conference on Communications (ICC)*, June 2020, pp. 1–6.

[36] L. Jensen and E. D. Carvalho, "An optimal channel estimation scheme for intelligent reflecting surfaces based on a minimum variance unbiased estimator," in *Proc. IEEE International Conference on Acoustics, Speech, and Signal Processing (ICASSP)*, 2020, pp. 5000–5004.

[37] Q. U. A. Nadeem, A. Chaaban, and M. Debbah, "Opportunistic beamforming using an intelligent reflecting surface without instantaneous CSI," *IEEE Wireless Communications Letters*, pp. 1–1, 2020.

[38] W. Tang, M. Z. Chen, X. Chen, J. Y. Dai, Y. Han, M. Di Renzo, Y. Zeng, S. Jin, Q. Cheng, and T. J. Cui, "Wireless Communications with Reconfigurable Intelligent Surface: Path Loss Modeling and Experimental Measurement," *arXiv e-prints*, p. arXiv:1911.05326, Nov 2019.

[39] S. W. Ellingson, "Path Loss in Reconfigurable Intelligent Surface-Enabled Channels," *arXiv e-prints*, p. arXiv:1912.06759, Dec. 2019.

[40] D. R. Smith, O. Yurduseven, L. P. Mancera, P. Bowen, and N. B. Kundtz, "Analysis of a waveguide-fed metasurface antenna," *Phys. Rev. Applied*, vol. 8, p. 054048, Nov 2017. [Online]. Available: https://link.aps.org/doi/10.1103/PhysRevApplied.8.054048

[41] C. Pfeiffer and A. Grbic, "Metamaterial Huygens' surfaces: Tailoring wave fronts with reflectionless sheets," *Phys. Rev. Lett.*, vol. 110, p. 197401, May 2013. [Online]. Available: https://link.aps.org/doi/10.1103/PhysRevLett.110.197401

[42] M. Selvanayagam and G. V. Eleftheriades, "Circuit modeling of Huygens surfaces," *IEEE Antennas and Wireless Propagation Letters*, vol. 12, pp. 1642–1645, 2013.

[43] N. Mohammadi Estakhri and A. Alù, "Wave-front transformation with gradient metasurfaces," *Phys. Rev. X*, vol. 6, p. 041008, Oct 2016. [Online]. Available: https://link.aps.org/doi/10.1103/PhysRevX.6.041008

[44] C. A. Balanis, *Antenna Theory: analysis and design*. New Jersey, USA: Wiley, 2016.

[45] V. Degli-Esposti, "A diffuse scattering model for urban propagation prediction," *IEEE Transactions on Antennas and Propagation*, vol. 49, no. 7, pp. 1111–1113, July 2001.

[46] V. Degli-Esposti, F. Fuschini, E. M. Vitucci, and G. Falciasecca, "Measurement and modelling of scattering from buildings," *IEEE Transactions on Antennas and Propagation*, vol. 55, no. 1, pp. 143–153, Jan 2007.

[47] E. Björnson and L. Sanguinetti, "Demystifying the power scaling law of intelligent reflecting surfaces and metasurfaces," in *2019 IEEE 8th International Workshop on Computational Advances in Multi-Sensor Adaptive Processing (CAMSAP)*, 2019, pp. 549–553.

[48] L. M. Correia and P. O. Frances, "Estimation of materials characteristics from power measurements at 60 GHz," in *5th IEEE International Symposium on Personal, Indoor and Mobile Radio Communications, Wireless Networks - Catching the Mobile Future.*, vol. 2, Sep. 1994, pp. 510–513 vol.2.

[49] J. Pascual-Garca, J. Molina-Garca-Pardo, M. Martnez-Ingls, J. Rodrguez, and N. Saurn-Serrano, "On the importance of diffuse scattering model parameterization in indoor wireless channels at mm-wave frequencies," *IEEE Access*, vol. 4, pp. 688–701, 2016.

Davide Dardari (S'96-M'99-SM'07) received the Laurea degree in electronic engineering (summa cum laude) and the Ph.D. degree in electronic engineering and computer science from the University of Bologna, Italy, in 1993 and 1998, respectively. Currently, he is an Associate Professor at the University of Bologna, Italy. Since 2005, he has been a Research Affiliate at Massachusetts Institute of Technology, USA. His interests are on wireless communications, localization techniques and distributed signal processing. He published more than 250 technical papers and played several important roles in various National and European Projects. He received the IEEE Aerospace and Electronic Systems Society's M. Barry Carlton Award (2011) and the IEEE Communications Society's Fred W. Ellersick Prize (2012).

He is Senior Member of the IEEE where he was the Chair for the Radio Communications Committee and Distinguished Lecturer (2018-2019) of the IEEE Communication Society. He was co-General Chair of the 2011 IEEE International Conference on Ultra-Wideband and co-organizer of the IEEE International Workshop on Advances in Network Localization and Navigation (ANLN) - ICC 2013-2016 editions. He was also TPC Chair of IEEE International Symposium on Personal, Indoor and Mobile Radio Communications (PIMRC 2018), TPC co-Chair of the Wireless Communications Symposium of the 2007/2017 IEEE International Conference on Communications, and TPC co-Chair of the 2006 IEEE International Conference on Ultra-Wideband. He served as an Editor for IEEE Transactions on Wireless Communications from 2006 to 2012 and as Guest Editor for several Journals.

Devis Massari received the Bachelor's degree in Electronics Engineering for Energy and Information (2017) and a Master's degree in Electronics and Telecommunications Engineering for Energy (2019) at the University of Bologna, Italy. Now he is a Software Engineer at J.M.A. Wireless - Teko Telecom Srl in Castel San Pietro (BO), Italy. His interests are on wireless communications and software design for 4G and 5G communication standards.